



PAPER • OPEN ACCESS

Finite-range effects in ultradilute quantum drops

To cite this article: V Cikojevi *et al* 2020 *New J. Phys.* **22** 053045

View the [article online](#) for updates and enhancements.



PAPER

Finite-range effects in ultradilute quantum drops

V Cikojević¹, L Vranješ Markić¹  and J Boronat^{2,3} ¹ Faculty of Science, University of Split, Ruđera Boškovića 33, HR-21000 Split, Croatia² Departament de Física, Universitat Politècnica de Catalunya, Campus Nord B4-B5, E-08034 Barcelona, Spain³ Author to whom any correspondence should be addressed.E-mail: jordi.boronat@upc.edu

Keywords: BEC gases, Bose mixtures, quantum Monte Carlo

RECEIVED

22 January 2020

REVISED

16 March 2020

ACCEPTED FOR PUBLICATION

3 April 2020

PUBLISHED

27 May 2020

Original content from
this work may be used
under the terms of the
[Creative Commons
Attribution 4.0 licence](https://creativecommons.org/licenses/by/4.0/).

Any further distribution
of this work must
maintain attribution to
the author(s) and the
title of the work, journal
citation and DOI.



Abstract

In the first experimental realization of dilute Bose–Bose liquid drops using two hyperfine states of ^{39}K some discrepancies between theory and experiment were observed. The standard analysis of the data using the Lee–Huang–Yang beyond mean-field theory predicted critical numbers which were significantly off the experimental measurements. Also, the radial size of the drops in the experiment proved to be larger than expected from this theory. Using a new functional, which is based on quantum Monte Carlo results of the bulk phase incorporating finite-range effects, we can explain the origin of the discrepancies in the critical number. This result proves the necessity of including finite-range corrections to deal with the observed properties in this setup. The controversy on the radial size is reasoned in terms of the departure from the optimal concentration ratio between the two species of the mixture.

1. Introduction

In the last years, there has been an increasingly high interest in understanding dilute, ultracold quantum Bose–Bose mixtures. The focus on this study increased dramatically after the theoretical proposal by Petrov [1] on the formation of self-bound liquid drops. These liquid drops are stabilized by beyond-mean-field effects and can appear in mixtures of two Bose–Einstein condensates with repulsive intraspecies and attractive interspecies interactions. The drops originate from a delicate balance between the collapsed state, predicted by mean-field (MF) theory, and the repulsive character of the first beyond mean-field term (Lee–Huang–Yang, LHY). The same perturbative theoretical scheme predicts self-binding in low-dimensional mixtures [2, 3] and dipolar systems [4, 5]. Recently, these predicted quantum drops have been observed in several experiments [6–9] and they resemble the well-known liquid Helium drops [10, 11]. However, the inner density in the Bose–Bose drops is about five orders of magnitude smaller than in ^4He [10, 11]. Therefore, these new quantum drops extend the realm of the liquid state to much lower densities than any previous existing classical or quantum liquid.

In the two labs [6, 8] where the drops have been observed, the Bose–Bose mixture is composed of two hyperfine states of ^{39}K . In the first experiment by Cabrera *et al* [6], the drops are harmonically confined in one of the directions of space whereas in the second one by Semeghini *et al* [8] the drops are observed in free space. This difference in the setup makes that in the first case the drops are not spherical like in the second experiment. This also affects the critical number, that is, the minimum number of atoms required to get a self-bound state. The measured critical numbers differ significantly between the two labs due to the different shape of the drops, the ones in the confined case being smaller than in the free case. In both works, the experimental results for the critical number are compared with the MF + LHY theory. The agreement between this theory and the drops produced in free space is quite satisfactory in spite of the large errorbars of the experimental data that hinder a precise comparison. However, in the confined drops of reference [6], where the critical numbers are significantly smaller than in the free case, the theoretical predictions do not match well the experimental data.

Ultradilute liquid drops, which require beyond-mean field corrections to be theoretically understood, offer the perfect benchmark to explore possible effects beyond MF + LHY theory [12] which usually play a minute role in the case of single-component gases [13, 14]. Indeed, several theoretical studies [15–19] indicate a strong dependence of the equation of state of the liquid on the details of the interatomic interaction, even at very low densities. This essentially means it is already possible to achieve observations outside the universal regime, in which all the interactions can be expressed in terms of the gas parameter na^3 , with a the s -wave scattering length. The first correction beyond this universality limit must incorporate the next term in the scattering series, that is the effective range r_{eff} [20, 21], which in fact can be quite large in these drops and in alkali atoms in general [22, 23].

Motivated by experiments with quantum drops, we have investigated the self-bound quantum mixture composed of two hyperfine states of ^{39}K using nonperturbative quantum Monte Carlo (QMC) methods. Direct QMC simulations [24] of finite particle-number drops, as produced in experiments, would serve as a great test of mean-field theory but, unfortunately, this is not yet achievable because of the large number of particles in realistic drops ($N > 10^4$). Yet, the problem can be addressed in the density functional theory (DFT) spirit, relying on the Hohenberg–Kohn–Sham 2nd theorem [25], which guarantees that a density functional exists that matches exactly the ground-state solution. To build a functional for the quantum Bose–Bose mixture, we have carried out calculations in bulk conditions using the diffusion Monte Carlo (DMC) method, an exact QMC technique applicable to systems at zero temperature. Using that functional we can access to energetics and structure of the liquid drops in the same conditions as in the experiment. We focus on the data obtained by Cabrera *et al* [6] in the confined setup since it is in that case where discrepancies between MF + LHY theory were observed.

The rest of the paper is organized as follows. In section 2, we introduce the theoretical methods used for the study and discuss the way in which the density functional is built. Section 3 comprises the results obtained for the bulk liquid using the available scattering data of the ^{39}K mixture. The inclusion of the effective range parameters in the interaction model allows for a better agreement with the measured critical numbers. Finally, we summarize the most relevant results here obtained and derive the main conclusions of our work.

2. Methods

We study a mixture of two hyperfine states of ^{39}K bosons at zero temperature. The Hamiltonian of the system is

$$H = \sum_{i=1}^N -\frac{\hbar^2}{2m} \nabla_i^2 + \frac{1}{2} \sum_{\alpha,\beta=1}^2 \sum_{i_{\alpha}j_{\beta}=1}^{N_{\alpha}N_{\beta}} V^{(\alpha,\beta)}(r_{i_{\alpha}j_{\beta}}), \quad (1)$$

where $V^{(\alpha,\beta)}(r_{i_{\alpha}j_{\beta}})$ is the interatomic potential between species α and β . The mixture is composed of $N = N_1 + N_2$ atoms, with N_1 (N_2) bosons of type 1 (2). The potentials are chosen to reproduce the experimental scattering parameters, and we have used different model potentials to investigate the influence of the inclusion of the effective range. The microscopic study has been carried out using a second-order DMC method [26], which allows for an exact estimation of the ground-state of the mixture within some statistical errors. DMC solves stochastically the imaginary-time Schrödinger equation using a trial wavefunction as importance sampling which guides the diffusion process to regions of expected large probability (see additional details on the DMC method in the appendix A). In the present case, we used a trial wavefunction built as a product of Jastrow factors [27],

$$\Psi(\mathbf{R}) = \prod_{i<j}^{N_1} f^{(1,1)}(r_{ij}) \prod_{i<j}^{N_2} f^{(2,2)}(r_{ij}) \prod_{i,j}^{N_1,N_2} f^{(1,2)}(r_{ij}), \quad (2)$$

where the two-particle correlation functions $f(r)$ are

$$f^{\alpha,\beta}(r) = \begin{cases} f_{2b}(r) & r < R_0 \\ B \exp\left(-\frac{C}{r} + \frac{D}{r^2}\right), & R_0 < r < L/2 \\ 1, & r > L/2. \end{cases} \quad (3)$$

The function f_{2b} is the solution of the two-body problem for a specific interaction model. This is connected to the long-range phonon wavefunction [27] with coefficients B , C and D , which are adjusted to match the continuity condition of the wavefunction, its first derivative, and the zero derivative at $r = L/2$. R_0 is the

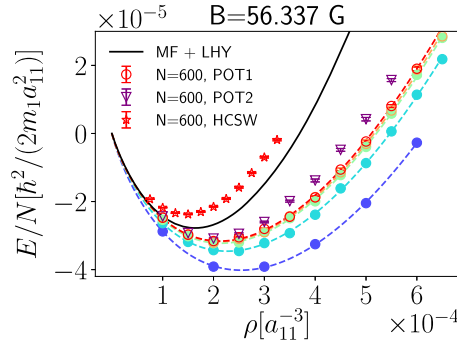


Figure 1. Dependence of the equation of state on the effective range for selected potential models, compared with MF + LHY. Full circles are calculations using POT1, and we illustrate the convergence to negligible finite-size effects starting from $N = 100$ (lower points), 200, 400, 500 to $N = 600$ (upper points). Dashed lines are fits to the DMC data with equation (11).

matching point to be variationally optimized, and $L = (N/\rho)^{1/3}$ is the size of the simulation box. Our study shows that there is a weak dependence of the variational energy on R_0 once scaled in L units, and thus it has been kept as $R_0 = 0.9L/2$ for all the cases. A careful analysis of imaginary time-step dependence and population size bias has been carried out, keeping both well under the statistical error.

Within density functional theory (DFT), we seek for a many-body wavefunction built as a product of single-particle orbitals,

$$\Psi(\mathbf{r}_1, \mathbf{r}_2, \dots, \mathbf{r}_N) = \prod_{i=1}^N \psi(\mathbf{r}_i). \quad (4)$$

These single-particle wavefunctions, which in general are time-dependent, are obtained by solving the Schrödinger-like equation [28],

$$i\hbar \frac{\partial \psi}{\partial t} = \left(-\frac{\hbar^2}{2m} \nabla^2 + V_{\text{ext}}(\mathbf{r}) + \frac{\partial \mathcal{E}_{\text{int}}}{\partial \rho} \right) \psi, \quad (5)$$

where V_{ext} is an external potential acting on the system and \mathcal{E}_{int} is an energy per volume term that accounts for the interparticle correlations. The differential equation (5) is solved by propagating the wavefunction ψ with the time-evolution operator

$$\psi(t + \Delta t) = e^{-iH\Delta t} \psi(t). \quad (6)$$

To this end, we have implemented a three-dimensional numerical solver based on the Trotter decomposition of the time evolution operator [29, 30] with second-order accuracy in the timestep Δt , as follows

$$e^{-iH\Delta t} = e^{-i\Delta t V(R)/2} e^{-i\Delta t K} e^{-i\Delta t V(R)/2} + \mathcal{O}(\Delta t^2), \quad (7)$$

with K and V the kinetic and potential terms in equation (5).

3. Results

In order to go beyond the MF + LHY density functional we have carried out DMC calculations of the bulk liquid. In the mixture of ^{39}K under study, we call the state $|F, m_F\rangle = |\downarrow\rangle = |1, 0\rangle$ as component 1, and the state $|F, m_F\rangle = |\uparrow\rangle = |1, -1\rangle$ as component 2. In figure 1, we show the energy per particle of the ^{39}K mixture as a function of the density, using three different sets of potentials in the Hamiltonian (1):

- Hard-core interactions (HCSW) with diameter a_{ii} , $i = 1, 2$, for the repulsive intraspecies interaction, and a square-well potential with range $R = a_{11}$ and depth V_0 for the interspecies potential. The three potentials reproduce the s -wave scattering lengths for the three channels,
- POT1 stands for a set of potentials which reproduces both the s -wave scattering lengths and effective ranges of the three interacting pairs of the ^{39}K mixture. To model the interactions, we have chosen a square-well square barrier potential [31] for the 11 channel, a 10–6 Lennard-Jones potential [32] for the 22 channel, and a square-well potential of range R and depth V_0 [13] in the 12 channel,
- POT2 also reproduce both the s -wave scattering lengths and effective ranges, by using a sum of Gaussians in the 11 channel, a 10–6 Lennard-Jones potential in the 12 channel, and finally a soft-sphere square well in the 22 channel.

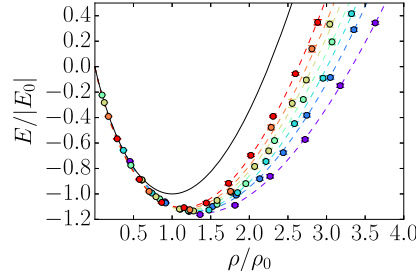


Figure 2. DMC energy per particle as a function of the density (circles), starting from $B = 56.230$ G (lower points) to $B = 56.639$ G (upper points). Energy and density are normalized to E_0 and ρ_0 , given in equations (9) and (10), respectively. Dashed lines are fits with equation (11). Full line is the MF + LHY theory (equation (8)).

In all cases, the attractive interatomic potential does not support a two-body bound state. We have obtained the s -wave scattering length and effective range of the potentials using standard scattering theory [20, 21]. More specific details of the model potentials are reported in the appendix A.

We compare our DMC results to the MF + LHY theory, which can be compactly written as [1]

$$\frac{E/N}{|E_0/N|} = -3 \left(\frac{\rho}{\rho_0} \right) + 2 \left(\frac{\rho}{\rho_0} \right)^{3/2}, \quad (8)$$

assuming the optimal concentration of particles from mean-field theory, $N_1/N_2 = \sqrt{a_{22}/a_{11}}$. The energy per particle E_0/N at the equilibrium density of the MF + LHY approximation ρ_0 and ρ_0 itself is

$$E_0/N = \frac{25\pi^2 \hbar^2 |a_{12} + \sqrt{a_{11}a_{22}}|^3}{768ma_{22}a_{11} (\sqrt{a_{11}} + \sqrt{a_{22}})^6}, \quad (9)$$

$$\rho_0 a_{11}^3 = \frac{25\pi}{1024} \frac{(a_{12}/a_{11} + \sqrt{a_{22}/a_{11}})^2}{(a_{22}/a_{11})^{3/2} (1 + \sqrt{a_{22}/a_{11}})^4}. \quad (10)$$

In figure 1, we report DMC results for the equation of state corresponding to a magnetic field $B = 56.337$ G, one of the magnetic fields used in experiments. We show the convergence of the results on the number of particles in the simulation for the particular case of POT1 set of potentials. As we can see, the convergence is achieved with $N = 600$. We have repeated this analysis for all the potentials and, in all the magnetic field range explored, we arrive to convergence with similar N values. We have investigated the dependence on the effective range by repeating the calculation using the HCSW and POT2 potentials. As it is clear from figure 1, only when both scattering parameters, the s -wave scattering length and the effective range, are imposed on the model potentials we get an approximate universal equation of state, mainly around the equilibrium density. The equation of state so obtained shows a significant and overall decrease of the energy compared to the MF + LHY prediction, with a correction that increases with the density. Instead, using the HCSW potentials, which only fulfill the s -wave scattering lengths, the energies obtained are even above the MF + LHY prediction. A similar behavior has been previously shown to hold in symmetric ($N_1 = N_2$) Bose–Bose mixtures [16].

Equations of state of the bulk mixture, for the seven values of the magnetic field used in the experiments ($B = 56.230$ G to $B = 56.639$ G), are shown in figure 2. The DMC results are calculated using the model POT1, but the differences with the other set POT2 are not significant. In all cases, we take the mean-field prediction for the optimal ratio of partial densities $\rho_1/\rho_2 = \sqrt{a_{22}/a_{11}}$. We have verified in several cases that this is also the concentration corresponding to the ground state of the system in our DMC calculations, i.e., the one that gives the minimum energy at equilibrium. The DMC results are compared with the MF + LHY equation of state (8). Overall, a reduction of the magnetic field, or equivalently an increase in $|\delta a| = a_{12} + \sqrt{a_{11}a_{12}}$, leads to an increase of the binding energy compared to the MF + LHY approximation. This happens clearly due to the influence of the large experimental effective range, since in the limit of zero range one would observe overall repulsive beyond-LHY terms (see also figure 1 and reference [16]).

DMC energies for the ^{39}K mixture are well fitted using the functional form

$$E/N = \alpha \rho + \beta \rho^\gamma, \quad (11)$$

as it can be seen in figure 2. These equations of state, calculated within the range of magnetic fields used in experiments, are then used in the functional form (5) with $\mathcal{E}_{\text{int}} = \rho E/N$. With the new functional, based on

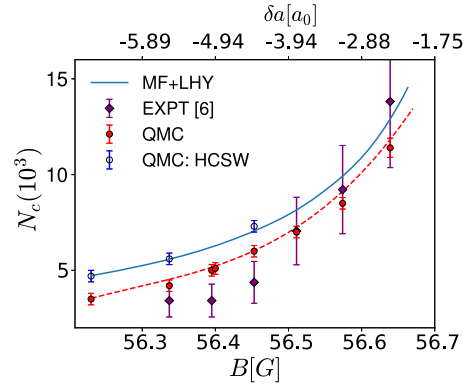


Figure 3. Dependence of the critical atom number on the magnetic field. Full circles are predictions using the QMC functional within DFT with the interaction potentials which reproduce both a and r_{eff} . Diamond points are data from the experiment [6]. Empty points show the prediction using the QMC functional with the HCSW model potentials.

Table 1. Critical atom number to form a droplet in a harmonic trap $V_z = \frac{1}{2}m\omega_z^2 z^2$, where $a_{\text{ho}} = \sqrt{\hbar/(m\omega_z)} = 0.639 \mu\text{m}$ is the same value as in the experiment [6]. $\varepsilon_r = |N_c^{\text{QMC}} - N_c^{\text{MFLHY}}|/N_c^{\text{MFLHY}}$ is the relative error.

$B(\text{G})$	N_c^{QMC}	N_c^{MFLHY}	ε_r	$N_c^{\text{QMC}} - N_c^{\text{MFLHY}}$
56.23	3500	4650	0.25	-1150
56.337	4200	5570	0.25	-1370
56.395	5000	6200	0.19	-1200
56.4	5100	6250	0.18	-1150
56.453	6000	7000	0.14	-1000
56.511	7000	8050	0.13	-1050
56.574	8500	9800	0.13	-1300
56.639	113 00	127 00	0.11	-1400

Table 2. Critical atom number for spherical free drops [8]. $\varepsilon_r = |N_c^{\text{QMC}} - N_c^{\text{MFLHY}}|/N_c^{\text{MFLHY}}$ is the relative error.

$B(\text{G})$	N_c^{QMC}	N_c^{MFLHY}	ε_r	$N_c^{\text{QMC}} - N_c^{\text{MFLHY}}$
56.23	160 00	158 00	0.01	200
56.337	246 00	249 00	0.01	-300
56.395	327 00	339 00	0.04	-1200
56.4	353 00	355 00	0.01	-200
56.453	472 00	477 00	0.01	-500
56.511	691 00	706 00	0.02	-1500
56.574	114 000	119 000	0.04	-5000
56.639	230 000	236 000	0.03	-6000

our DMC results, we can study the quantum drops with the proper number of particles which is too large for a direct DMC simulation.

Results for the critical atom number N_c at different B are shown in figure 3 in comparison with the experimental results of reference [6]. To make the comparison reliable, we have included the same transversal confinement as in the experiment. In particular, theoretical predictions are obtained within DFT, using a Gaussian ansatz $\phi = \exp(-r^2/(2\sigma_r^2) - z^2/(2\sigma_z^2))$. When the equation of state of the bulk takes into account the effective range of all the pairs we observe an overall decrease of N_c with respect to the MF + LHY prediction. Interestingly, if we use the HCSW model potentials, with essentially zero range, our results are on top of the MF + LHY line (see the points at $B = 56.23 \text{ G}$, $B = 56.337 \text{ G}$ and $B = 56.453 \text{ G}$ in figure 3). The observed decrease of N_c leads our theoretical prediction closer to the experimental data in a significant amount and in all the δa range, clearly showing the significant influence of the effective range on the N_c values. Experiments on quantum droplets were performed either in the harmonic trap [6] or in a free-drop setup [8]. Predictions of N_c for these two geometries are given in tables 1 and 2, using MF + LHY and QMC functionals. The absolute difference of predicted N_c values between the two functionals are about 1000 atoms. On the other hand, the relative difference is much higher in the harmonically-trapped system because the presence of an external trap significantly reduces N_c .

A second observable measured in experiments is the size of the drops. The radial size of a $N = 15\,000$ drop for different values of the magnetic field was reported in reference [6]. In figure 4, we compare the experimental values with different theoretical predictions. We observe a slight reduction in size using QMC

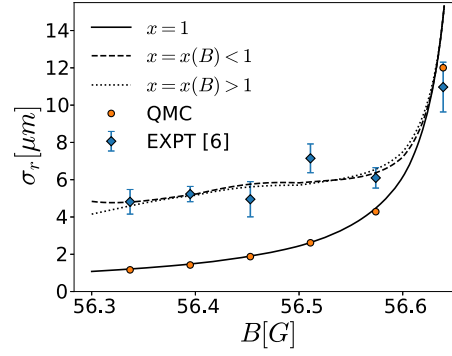


Figure 4. Dependence of the radial size of a $N = 15\,000$ drop on the external magnetic field, or equivalently the residual s -wave scattering length. Lines are predictions under MF + LHY theory; full line is a prediction with $x = 1$, dashed and dotted lines are fits of experimental sizes using a parameter x .

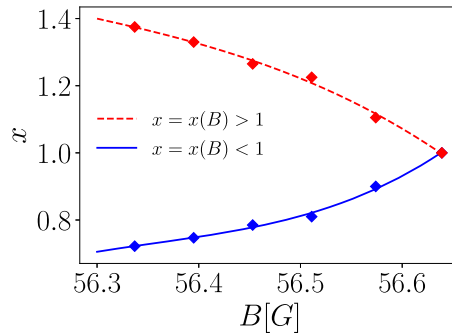


Figure 5. Values of $x = N_2/N_1 \sqrt{a_{22}/a_{11}}$ which reproduce the experimental size of a $N = 15\,000$ drop (figure 4) within the MF + LHY theory, as a function of the magnetic field. Points are the values which reproduce the size, and lines are power-law fits of x as a function of the magnetic field B . Note that two solutions exist since the choice of naming each component is twofold.

functionals, compared to MF + LHY theory, which is a consequence of the stronger binding produced by inclusion of finite range interactions. Since the experimental data go to the opposite direction, it means that drops size can not be explained solely in terms of the non-zero effective range. One possible explanation for this clear disagreement could be a deviation from the optimal relative number of particles, which can occur in non-equilibrated drops or when one of the components has a large three-body recombination coefficient. Let us define $x = N_2/N_1 \sqrt{a_{22}/a_{11}}$. Then, $x = 1$ stands for the optimal relative particle number, i.e., the concentration corresponding to the ground-state of the system. We have investigated the behavior of both the MF + LHY and QMC functionals under variations in x , and both predict an increase in the drop size proportional to the deviation from $x = 1$. Using the MF + LHY functional, we have obtained the x values that fit the experimental size for every B (figure 4). We report the result of this analysis in figure 5; notice that there is a symmetry on x and so only its absolute deviation from one is important. This result clearly shows the sensitive dependence of drop structural properties on the relative atom number. We also carried out a similar analysis in the case of the spherical drops obtained in reference [8]. In that case, it is observed that both the MF + LHY and QMC results with $x = 1$ are compatible with the measured sizes within the (large) experimental error bars. Therefore, it seems that the transversally confined drops are more sensitive to the value of x , probably because they are not spherical and their size can only grow in two directions of space instead of three.

As we can see in figure 5, the value for x becomes 1 (optimal value) when the drop composed by 15 000 particles is studied at the highest magnetic field. This can be understood if we observe that the critical number for this magnetic field matches approximately this number of atoms (see figure 3). When the number of atoms of a drop is larger than the critical number (lower B in figure 4) x departs from one. This can be better understood if one calculates the drop phase diagram as a function of x . The result is plotted in figure 6. As the number of particles is approaching the critical one, the range of possible values of x , which support a drop state, is reducing. This is a supporting fact that drops close to the critical atom number observed in the experiment fulfill the condition $x = 1$. On the other hand, there is an increasing range of relative particle concentrations for which a drop can emerge as the number of particles increases.

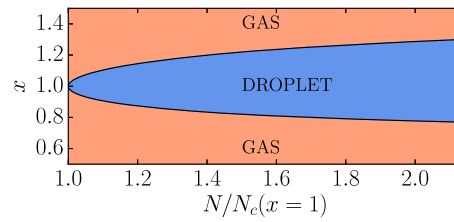


Figure 6. Phase diagram of ^{39}K at $B = 56.230$ G using MF + LHY theory, spanned with $x = N_2/N_1 \sqrt{a_{22}/a_{11}}$ and the total particle number N , normalized with the critical atom number N_c evaluated at $x = 1$ [1].

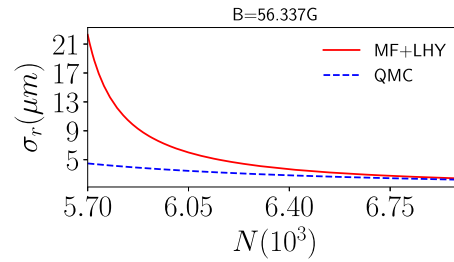


Figure 7. Dependence of the radial size σ_r on the number of particles. The size is obtained from the variational ansatz, since close to the critical atom number the density profile in the radial direction is well approximated by a Gaussian. In both functionals, it is assumed that the relative concentration is optimal $N_2/N_1 = \sqrt{a_{11}/a_{22}}$. QMC functional includes the correct finite-range r_{eff} through POT1 set of potentials, figure 1.

Close to the critical atom number, the density profile of a drop can change drastically depending on the functional. We illustrate this effect in figure 7 for a magnetic field $B = 56.337$ G. In the figure, we show the dependence of the radial size on the number of particles, with the same harmonic confinement strength as in one of the experiments [6]. We observe a substantial difference between the MF + LHY and QMC functional results, mainly when N approaches the critical number N_c .

4. Discussion

Experiment in reference [6] showed a significant disagreement between the measured data and the MF + LHY perturbative approach. In order to determine the possible origin of these discrepancies we have pursued a beyond MF + LHY theory which incorporates explicitly the finite range of the interaction. To this end, we have carried out DMC calculations of the bulk liquid to estimate accurately its equation of state. We have observed that the inclusion in the model potentials of both the s -wave scattering length and the effective range produces a rather good universal equation of state in terms of these pair of parameters. Excluding the effective range, significant differences are obtained from these universal results. This relevant result points to the loss of universality in terms of the gas parameter in the study of these dilute liquid drops.

Introducing the DMC equation of state into the new functional, following the steps which are standard in other fields, such as DFT in liquid helium [10], we derive a new functional that allows for an accurate study of the most relevant properties of the drops. In particular, we observe that the inclusion of finite range effects reduces the critical atom number in all the magnetic field range approaching significantly the experimental values. On the other hand, our QMC functional is not able to explain the clear discrepancy between theory and experiment about the size of the drops. We attribute this difference to the dramatic effect on the size that small shifts on the value of x produce. Our analysis provides a reasonable explanation of this feature: above the critical atom number the window of stability of the drops increases from the single point $x = 1$ to a range of values that, in absolute terms, grow with the number of particles. With the appropriate choice of x , one can obtain agreement with the experiment.

The drops produced in the different setup of reference [8] are spherical since all magnetic confinement is removed. The corresponding critical numbers in this case are larger than in the confined setup [6] and MF + LHY theory accounts reasonably well for the observed features. We have applied our formalism also to this case and the corrections are not zero but relatively less important than in the case analyzed here.

Acknowledgments

We acknowledge very fruitful discussions with Leticia Tarruell, César Cabrera, and Julio Sanz. This work has been supported by the Ministerio de Economía, Industria y Competitividad (MINECO, Spain) under Grant No. FIS2017-84114-C2-1-P. V C acknowledges financial support from STSM Grant COST Action CA16221.

Appendix A

A.1. Diffusion Monte Carlo

The diffusion Monte Carlo (DMC) method provides exact energy for Bose systems at zero temperature, within some statistical noise [26]. The starting point of the DMC method is the N -body Schrödinger equation written in imaginary time $\tau = -it$

$$-\frac{\partial \Psi}{\partial \tau} = \hat{H}\Psi, \quad (12)$$

with \hat{H} the Hamiltonian of the system. To reduce the variance, one uses importance sampling by solving the Schrödinger equation. This is made by introducing the wavefunction $f = \psi_T \phi$, where ϕ is the ground-state many-body wavefunction and ψ_T is a trial wavefunction. The trial wavefunction that we use (equations (2) and (3)) reproduces the expected behavior at small and large distance between atom pairs, thus focusing the sampling where it is physically most likely. The wavefunction f is represented numerically by a set of *walkers*, different coordinate configurations of f , and it evolves in time as

$$-\frac{\partial f}{\partial \tau} = -\frac{\hbar^2}{2m} \nabla^2 f - \frac{\hbar^2}{2m} \nabla (Ff) + (E_L(\mathbf{R}) - E_{\text{ref}})f, \quad (13)$$

where $F = \psi_T^{-1} \nabla \psi_T$, $E_L = \psi_T^{-1} \hat{H} \psi_T$ and E_{ref} is the reference energy used to stabilize the DMC simulation. We employ the short-time Trotter decomposition up to second order in the timestep to iterate the equation (13) [26]. There are several biases in the DMC method, which are reduced when (i) the simulation time is large enough, (ii) the number of walkers is large enough, and (iii) when the time-step is small enough. In our study, the time-step dependence is well eliminated for $\Delta\tau = 0.2 \times ma_{11}^2/\hbar$ and the population bias by using $n_w = 100$ walkers. Thus, the error estimates that we report come only from the inherent statistical noise of Monte Carlo simulations. The calculations of the bulk liquid are performed in a simulation box with periodic boundary conditions. We have studied the convergence to the thermodynamic limit by performing a set of calculations with different total atom numbers, for a given fixed density. Convergence of the energy per particle is achieved for $N \approx 600$ for all the magnetic fields.

A.2. Interaction potentials

For the system under study, ^{39}K , we only know two scattering parameters, that is the s -wave scattering length and the effective range. In order to model the interaction potentials with those parameters, we have used three different set of potentials. Notice that, for a given set of just two scattering parameters, there is an uncountable number of corresponding potentials. We have used the HCSW potentials to investigate mixtures only in the limit of zero range. However, this set of potentials cannot reproduce the scattering parameters of ^{39}K given in table 3. In order to fulfill both scattering conditions, s -wave scattering lengths and effective ranges, the interaction potentials need to have a more elaborate shape. To this end, we use the POT1 and POT2 set of potentials (figure A.1). These particular choices of interaction models are somewhat arbitrary, since we have focused only on reproducing two scattering parameters, but they are able to match the experimental scattering parameters in all the channels. On the other hand, all the potentials that we use do not support a two-body bound state.

A.3. HCSW potentials

In the HCSW set of potentials, intraspecies repulsion is modeled by the hard-core interaction

$$V_{ii}(r) = \begin{cases} \infty, & r < a_{ii} \\ 0, & r \geq a_{ii} \end{cases} \quad (14)$$

for $i = 1, 2$. The s -wave scattering length of this potential corresponds to the diameter of the hard core. Interspecies attraction is modeled by the attractive square well potential

Table 3. Scattering parameters [33], s -wave scattering length a and the effective range r^{eff} in units of Bohr radius a_0 , as a function of the magnetic field B .

$B(\text{G})$	$a_{11}(a_0)$	$r_{11}^{\text{eff}}(a_0)$	$a_{22}(a_0)$	$r_{22}^{\text{eff}}(a_0)$	$a_{12}(a_0)$	$r_{12}^{\text{eff}}(a_0)$
56.230	63.648	−1158.872	34.587	578.412	−53.435	1021.186
56.337	66.619	−1155.270	34.369	588.087	−53.386	1022.638
56.395	68.307	−1153.223	34.252	593.275	−53.360	1022.617
56.400	68.453	−1153.046	34.242	593.722	−53.358	1022.616
56.453	70.119	−1150.858	34.136	599.143	−53.333	1023.351
56.511	71.972	−1148.436	34.020	604.953	−53.307	1024.121
56.574	74.118	−1145.681	33.895	610.693	−53.278	1024.800
56.639	76.448	−1142.642	33.767	616.806	−53.247	1025.593

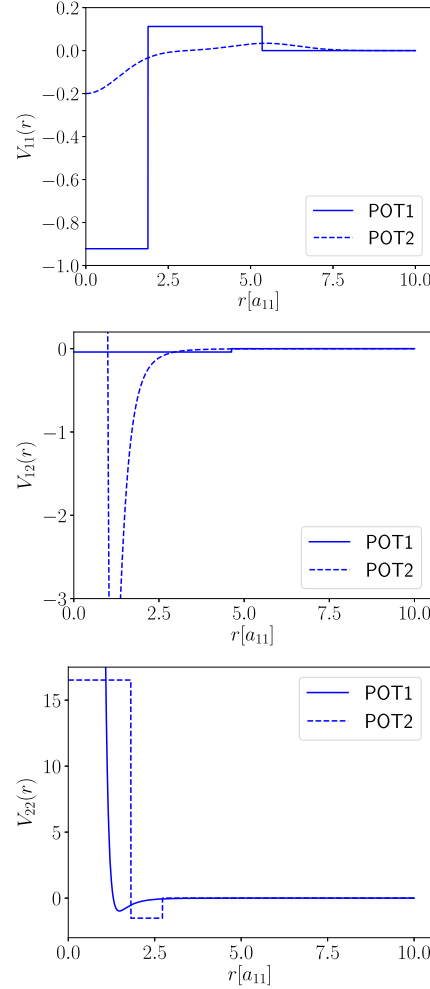


Figure A.1. POT1 and POT2 potentials in each of the channels which reproduce the s -wave scattering lengths and effective ranges for $B = 56.337$ G.

$$V_{12}(r) = \begin{cases} -V_0, & r < R_0 \\ 0, & r \geq R_0 \end{cases} \quad (15)$$

The s -wave scattering length and effective range of the attractive square well can be found in reference [13].

A.4. POT1 potentials

For the POT1 set of potentials, we use the following

$$V_{11}(r) = \begin{cases} -V_0, & r < R_0 \\ V_1, & R_0 \leq r < R_1 \\ 0, & r \geq R_1 \end{cases} \quad (16)$$

$$V_{12}(r) = \begin{cases} -V_0, & r < R_0 \\ 0, & r \geq R_0 \end{cases} \quad (17)$$

$$V_{22}(r) = V_0 \left[\left(\frac{r_0}{r} \right)^{10} - \left(\frac{r_0}{r} \right)^6 \right] \quad (18)$$

The scattering parameters in the 11 channel can be found in reference [31], in the 12 channel in reference [13], and in the 22 one in reference [32]. The effective range of the 12 potential was found numerically by solving the two-body scattering problem [20].

A.5. POT2 potentials

For the POT2 set of potentials, we use the following

$$V_{11}(r) = -V_0 \exp \left[-\frac{r^2}{2r_0^2} \right] + V_1 \exp \left[-\frac{(r-r_1)^2}{2r_0^2} \right] \quad (19)$$

$$V_{12}(r) = V_0 \left[\left(\frac{r_0}{r} \right)^{10} - \left(\frac{r_0}{r} \right)^6 \right] \quad (20)$$

$$V_{22}(r) = \begin{cases} V_0, & r < R_0 \\ -V_1, & R_0 \leq r < R_1 \\ 0, & r \geq R_1 \end{cases} \quad (21)$$

The scattering parameters for the potential in the 11 channel are found numerically [20]; the ones for the 22 channel can be obtained from reference [31].

ORCID iDs

L Vranješ Markić  <https://orcid.org/0000-0002-4912-3840>

J Boronat  <https://orcid.org/0000-0002-0273-3457>

References

- [1] Petrov D S 2015 *Phys. Rev. Lett.* **115** 155302
- [2] Petrov D S and Astrakharchik G E 2016 *Phys. Rev. Lett.* **117** 100401
- [3] Parisi L, Astrakharchik G E and Giorgini S 2019 *Phys. Rev. Lett.* **122** 105302
- [4] Kadau H, Schmitt M, Wenzel M, Wink C, Maier T, Ferrier-Barbut I and Pfau T 2016 *Nature* **530** 194
- [5] Bombin R, Boronat J and Mazzanti F 2017 *Phys. Rev. Lett.* **119** 250402
- [6] Cabrera C R, Tanzi L, Sanz J, Naylor B, Thomas P, Cheiney P and Tarruell L 2018 *Science* **359** 301
- [7] Cheiney P, Cabrera C R, Sanz J, Naylor B, Tanzi L and Tarruell L 2018 *Phys. Rev. Lett.* **120** 135301
- [8] Semeghini G, Ferioli G, Masi L, Mazzinghi C, Wolswijk L, Minardi F, Modugno M, Modugno G, Inguscio M and Fattori M 2018 *Phys. Rev. Lett.* **120** 235301
- [9] D'Errico C, Burchianti A, Prevedelli M, Salasnich L, Ancilotto F, Modugno M, Minardi F and Fort C 2019 arXiv:1908.00761v2
- [10] Barranco M, Guardiola R, Hernández S, Mayol R and Pi M 2006 *J. Low Temp. Phys.* **142** 1
- [11] Chin S A and Krotscheck E 1995 *Phys. Rev. B* **52** 10405
- [12] Jørgensen N B, Bruun G M and Arlt J J 2018 *Phys. Rev. Lett.* **121** 173403
- [13] Pethick C J and Smith H 2008 *Bose–Einstein Condensation in Dilute Gases* (Cambridge: Cambridge University Press)
- [14] Giorgini S, Boronat J and Casulleras J 1999 *Phys. Rev. A* **60** 5129
- [15] Staudinger C, Mazzanti F and Zillich R E 2018 *Phys. Rev. A* **98** 023633
- [16] Cikojević V, Vranješ Markić L, Astrakharchik G E and Boronat J 2019 *Phys. Rev. A* **99** 023618
- [17] Tononi A 2019 *Condens. Matter* **4** 20
- [18] Tononi A, Cappellaro A and Salasnich L 2018 *New J. Phys.* **20** 125007
- [19] Salasnich L 2017 *Phys. Rev. Lett.* **118** 130402
- [20] Newton R G 1982 *Scattering Theory of Waves and Particles* (New York, NY: Springer)
- [21] Roman P 1965 *Advanced Quantum Theory* (Reading, MA: Addison-Wesley)
- [22] Flambaum V V, Gribakin G F and Harabati C 1999 *Phys. Rev. A* **59** 1998
- [23] Tanzi L, Cabrera C R, Sanz J, Cheiney P, Tomza M and Tarruell L 2018 *Phys. Rev. A* **98** 062712
- [24] Cikojević V, Dželalija K, Stipanović P, Vranješ Markić L and Boronat J 2018 *Phys. Rev. B* **97** 140502
- [25] Hohenberg P and Kohn W 1964 *Phys. Rev.* **136** B864
- [26] Boronat J and Casulleras J 1994 *Phys. Rev. B* **49** 8920
- [27] Reatto L and Chester G V 1967 *Phys. Rev.* **155** 88
- [28] Ancilotto F, Barranco M, Guilleumas M and Pi M 2018 *Phys. Rev. A* **98** 053623
- [29] Chin S A, Janecek S and Krotscheck E 2009 *Chem. Phys. Lett.* **470** 342
- [30] Pi M and Barranco M private communication
- [31] Jensen L M, Nilsen H M and Watanabe G 2006 *Phys. Rev. A* **74** 043608
- [32] Pade J 2007 *Eur. Phys. J. D* **44** 345
- [33] Roy S, Landini M, Trenkwalder A, Semeghini G, Spagnolli G, Simoni A, Fattori M, Inguscio M and Modugno G 2013 *Phys. Rev. Lett.* **111** 053202